Chinese Chemical Letters 34 (2023) 107239

Contents lists available at ScienceDirect

Chinese Chemical Letters

journal homepage: www.elsevier.com/locate/cclet

Surface charge transfer doping of graphene using a strong molecular dopant CN6-CP

Xiaojuan Dai[a], Liyao Liu[a], Zhen Ji[a,b], Qing Meng[a], Ye Zou[a,*]

[a] Beijing National Laboratory for Molecular Sciences, CAS Key Laboratory of Organic Solids, Institute of Chemistry, Chinese Academy of Sciences, Beijing 100190, China
[b] School of Chemical Sciences, University of Chinese Academy of Sciences, Beijing 100049, China

ARTICLE INFO

Article history:
Received 9 February 2022
Revised 14 February 2022
Accepted 16 February 2022
Available online 19 February 2022

Keywords:
Graphene
Surface charge transfer doping
Molecular dopant
CN6-CP
Hall effect

ABSTRACT

Surface charge transfer doping of graphene plays an important role in graphene-based electronics due to its simplicity, high doping efficiency, and easy-controllability. Here, we demonstrate the effective surface charge transfer hole doping of graphene by using a strong p-type molecular dopant hexacyanotrimethylene-cyclopropane (CN6-CP). The CN6-CP exhibits a very high intrinsic work function of 6.37 eV, which facilitates remarkable electron transfer from graphene to CN6-CP as revealed by *in situ* photoelectron spectroscopy investigations. Consequently, hole accumulation appears in the graphene layer at the direct contact with CN6-CP. As evidenced by Hall effect measurements, the areal hole density of graphene significantly increased from 8.3×10^{12} cm^{-2} to 2.21×10^{13} cm^{-2} upon 6 nm CN6-CP evaporation. The CN6-CP acceptor with strong p-doping effect has great implications for both graphene-based and organic electronics.

Graphene has attracted extensive research attention due to its unique chemical and electronic properties, including superior carrier transport properties, high light transmission over a wide spectral range, excellent mechanical property and flexibility, and well chemical durability [1–5]. Owing to these outstanding advantages, graphene has shown great promise in high-performance and flexible electronic and optoelectronic applications, which includes but not limits to charge injection/transport layer [6,7], energy-conversion or energy-storage devices [8–10], and transparent conductive electrodes [11,12]. More importantly, the distinctive energy band structure of graphene provides a possibility and opportunity for the development of new principle (opto)electronic devices [13,14].

Doping of graphene is an important way to exploit its unique performance. The widely applied doping methods of graphene include the electrostatic doping [15], lattice doping [16–18], and surface charge transfer doping [19–22]. Typical electrostatic doping involves constructing graphene-based field-effect transistors to modulate the carrier type and concentration *via* gate bias [15], which is only applicable to limited specific devices. While the lattice doping donates additional electrons or holes into the graphene lattice by introducing heteroatoms to replace some of the carbon atoms [17], which will also result in lattice structural defects and carrier scattering centers, leading to reduced carrier mobility. By contrast, the surface charge transfer doping by forming a surface contact with charge-transfer interaction between the dopant and graphene can be utilized to manipulate the electronic properties and work function of graphene simply and effectively [19], thereby exhibiting distinct applications in graphene-based optoelectronic devices. Numerous dopants including metals [23,24], transition metal oxides or compounds [25–28], strong acids or bases [11,29], and organic molecules with electron donating or accepting groups [20,21,30], have been widely investigated for surface charge transfer doping of graphene. Among those surface charge transfer dopants, only limited molecular dopants were reported with strength doping ability. For further development of graphene electronics, discovering or developing more molecular dopants with strong electron donation or acceptance capability is highly desired.

Here, we demonstrate efficient surface charge transfer p-type doping of graphene by using a recently rediscovered strong molecular electron acceptor, hexacyano-trimethylene-cyclopropane (CN6-CP). The molecular structure of CN6-CP is shown in Fig. 1a. Although the CN6-CP was firstly synthesized as early as 1976 [31,32], its application as a molecular dopant in open literature was not explored until 2016 [33]. Its deep lowest unoccupied molecular orbital (LUMO) level of −5.87 eV facilitates strength p-doping of organic semiconductors even with deep highest oc-

* Corresponding author.
E-mail address: zouye@iccas.ac.cn (Y. Zou).

https://doi.org/10.1016/j.cclet.2022.02.044
1001-8417/

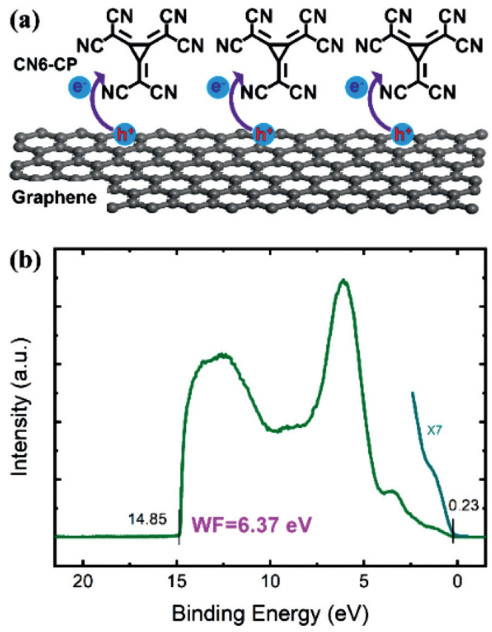

Fig. 1. (a) Molecular structure of CN6-CP and the illustration of doping mechanism. (b) UPS spectrum of 2 nm CN6-CP on bare Si substrate.

cupied molecular orbital (HOMO) levels, making CN6-CP dopant promising for applications in organic light-emitting diodes [34,35], thermoelectrics [36–39], and highly-conductive materials [33]. Attempts have also been made to develop its solution-processable derivatives or methods for broadening its applicability [40–42]. Modifying the graphene surface with CN6-CP is therefore expected to favor electron transfer from graphene into CN6-CP, leading to hole accumulation in graphene and thereby achieving p-type doping of graphene. The efficient hole doping of graphene is certified by both photoelectron spectroscopy and Hall effect analyses.

The few layer graphene on both Si and sapphire substrates were purchased from Anqing Gezhi Materials Company of China. Here, the graphene on Si substrates were used for ultraviolet and X-ray photoelectron spectroscopy (UPS and XPS) analyses, while the graphene on sapphire substrates were utilized for Hall effect measurements. The CN6-CP was synthesized following the reported procedure [33]. The UPS and XPS experiments were carried out in a Kratos AXIS Ultra DLD ultrahigh vacuum photoelectron spectroscopy connected to a custom-made high vacuum thermal evaporation system [43–45]. The base pressure of the analysis chamber and evaporation chamber were better than 5×10^{-10} and 5×10^{-9} Torr, respectively. The CN6-CP was thermally evaporated onto bare Si or graphene/Si substrates and immediately transferred to the analysis chamber without breaking the vacuum for UPS and XPS analyses. The deposition rate and film thickness of CN6-CP were *in-situ* monitored by a calibrated quartz crystal microbalance sensor (STM-2XM, Syncon Instrument). The UPS and XPS measurements were performed with an unfiltered He-discharge lamp ($h\nu = 21.22$ eV) and a monochromatic Al K_α X-ray ($h\nu = 1486.6$ eV) as the excitation sources, respectively. The samples were biased at −9.0 V to enable observation of secondary electron cut-off (SECO) for UPS spectra. The Fermi level (E_F) was calibrated from a UPS spectrum of sputtered clean (Ar^+ ion) Au substrate and was referred as the zero binding energy (E_B) in all the UPS and XPS spectra. The Hall effect experiments were carried out in a physical property measurement system (PPMS DynaCool-9T, Quantum Design) connected with a Keysight B2902A source unit for applying the excitation current and an Agilent 2182A nanovoltmeter for monitoring the real-time Hall voltage.

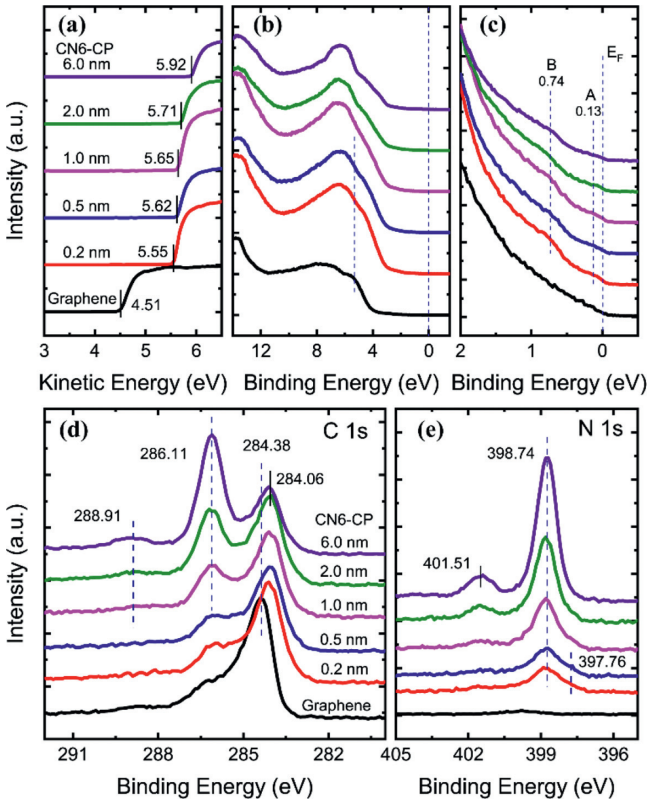

Fig. 2. UPS spectra of (a) SECO at the low kinetic energy region, (b) valence band feature at the low binding energy region and (c) the corresponding close-up spectra near E_F, and XPS core levels of (d) C 1s and (e) N 1s spectra during the successive deposition of CN6-CP on graphene.

We re-examined the electronic structure of CN6-CP by characterizing the UPS spectrum of a *quasi in-situ* thermally evaporated 2 nm CN6-CP on bare Si substrate with a native oxide surface layer. As shown in Fig. 1b, the UPS spectrum of pristine CN6-CP thin film displays an SECO position (E_{SECO}) or vacuum level at E_B of 14.85 eV, which indicates a rather high work function (WF) of 6.37 eV followed by: $WF = h\nu - E_{SECO}$. To the best of our knowledge, this WF is the highest value for the ever-reported organic molecules. Such a high WF should facilitate very efficient electron extraction from other materials in contact and thereby make CN6-CP a strong p-dopant.

The charge transfer at graphene/CN6-CP interface was monitored by the evolution of CN6-CP thickness-dependent UPS spectra of graphene. In order to intuitively show the change of WF, here we plot the SECO region with kinetic energy (E_K) coordinate, which is obtained by subtracting the E_B from $h\nu$: $E_K = h\nu - E_B$ (Fig. 2a) [46]. Originally, the vacuum level or SECO position of pristine graphene locates at E_K of 4.51 eV. Upon deposition of 0.2 nm CN6-CP, the vacuum level rapidly moves toward higher E_K by 1.04 eV, which indicates a rapid WF change from 4.51 eV to 5.55 eV. The remarkable upward shift of vacuum level or increase of WF indicates an efficient electron transfer from the graphene underlayer to the adsorbate CN6-CP, resulting in hole accumulation/doping in graphene (Fig. 1a) and formation of a prominent interface dipole. With increasing coverage of CN6-CP, a further gradual shift of the vacuum level towards higher E_K region can be observed, which shows a final position of 5.92 eV for 6.0 nm CN6-CP on graphene. Concurrently, the valance band feature of graphene also moves toward lower E_B region upon CN6-CP deposition (Fig. 2b). This is consistent with the p-doping effect of graphene by CN6-CP. Notably, two new weak peaks appear at E_B

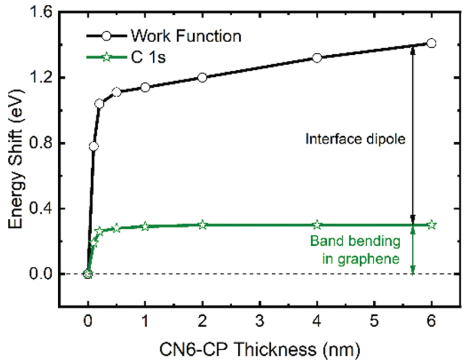

Fig. 3. Change of sample work function and sp^2 C 1s peak of graphene as a function of the CN6-CP coverage.

of about 0.13 eV (peak A) and 0.74 eV (peak B) in the valance band region near E_F (Fig. 2c). Since the valance band feature of pristine CN6-CP does not exist such two peaks (low E_B region in Fig. 1b) [34], they can not be simply ascribed to HOMO feature of CN6-CP. Virtually, similar phenomenon has been observed in other doped systems of both graphene and organic semiconductors [20,47,48]. Therefore, peak A in Fig. 2c can be assigned to the (partially) filled LUMO and peak B to the relaxed HOMO of CN6-CP after gaining electrons from graphene. Both peaks gradually attenuate at higher CN6-CP thickness, accompanied by the weak change of sample WF or vacuum level (Fig. 2a), indicating that the electron transfer primarily occurs at the graphene/CN6-CP interface.

Mechanism corresponding to the surface charge transfer doping was further explored by analyzing the interfacial chemical changes with XPS [49]. The representative XPS core level spectra of C 1s and N 1s as a function of CN6-CP thickness on graphene are presented in Figs. 2d and e. The pristine graphene shows a sp^2 dominated C 1s peak at 284.38 eV and a shoulder peak at 286.25 eV (Fig. 2d). The shoulder peak can be ascribed to the component of oxidation state or impurity. However, this peak does not affect the evaluation on graphene doping. After deposition of CN6-CP, a gradual shift of characteristic sp^2 C 1s peak of graphene toward lower E_B is observed. This is accompanied by the upward band-bending due to hole accumulation inside or p-type doping of graphene upon CN6-CP deposition. At higher CN6-CP thickness, the typical sp^2 C 1s feature of graphene is gradually attenuated and the typical C 1s component of CN6-CP appears at 286.11 eV with a shakeup peak at 288.91 eV. On the other hand, distinct N 1s feature, which can be splitted into two main peaks with their centers at 398.74 eV and 397.76 eV, respectively, appears when CN6-CP first comes into contact with graphene (Fig. 2e). The 398.74 eV portion belongs to neutral N 1s feature of CN6-CP, while the 397.76 eV portion is assigned to the negatively charged CN6-CP where significant charge transfer occurs in direct contact with graphene [20]. Further increasing CN6-CP thickness leads to a gradual attenuation of the 397.76 eV peak and a rapid increase of 398.73 eV peak, accompanied by the appearance of shakeup feature at 401.51 eV. The variations of both C 1s and N 1s spectra again reveal the electron transfer from graphene to CN6-CP primarily occurs at their interface.

The interfacial charge separation during the surface charge transfer doping results in an interface dipole, which in addition to the band bending contributes to the change of WF [50]. Therefore, the interface dipole can be derived by deducting the band bending from the change of WF. The energy changes of both sample WF and characteristic sp^2 C 1s peak of graphene as a function of CN6-CP thickness are plotted in Fig. 3. At the initial deposition of 0.2 nm CN6-CP, owing to the prominent energy difference between WF of graphene and CN6-CP, electrons spontaneously transfer from graphene to CN6-CP and holes are doped into the graphene layer.

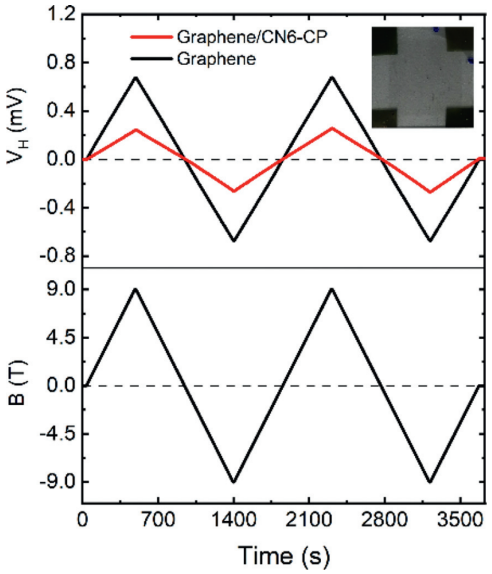

Fig. 4. Hall voltage response of the graphene van der Paul device before and after 6 nm CN6-CP evaporation.

Consequently, both the sample WF and sp^2 C 1s peak change rapidly, where the variation of WF is much larger than the shift of graphene C 1s. The CN6-CP at 0.2 nm is discontinuous, and as the thickness of CN6-CP increases, more CN6-CP molecules can be in contact with graphene. Therefore, these energy shift continues, but become slower with further increasing the CN6-CP coverage, which is because the strong charge transfer interaction between graphene and the subsequently deposited CN6-CP happens at their contact interface region and the bulk CN6-CP has a weaker effect. A total increase of 1.41 eV in sample WF and shift of 0.32 eV in graphene sp^2 C 1s peak are observed after deposition of 6.0 nm CN6-CP, indicating a large dipole of 1.09 eV formed at graphene/CN6-CP interface.

To further verify the strength p-doping effect of CN6-CP to graphene, we carried out Hall effect measurements on the same graphene device without and with CN6-CP deposition. The Hall device was fabricated with a van der Paul geometry as shown in inset of Fig. 4. Here, Au contacts are thermally evaporated by a shadow mask onto the four corners of a square graphene with a side length of 7 mm. A DC excitation current (I) of 1 μA was applied to one set of the diagonal electrodes through the sample and the transverse Hall voltage (V_H) was measured from the other set of diagonal electrodes by the Fleming's left-hand rule during a magnetic field (B) sweep between −9 T and 9 T at room temperature [51]. The Hall voltage response of the graphene Hall devices before and after 6 nm CN6-CP deposition are depicted in Fig. 4, which shows a linear development of Hall voltage with the magnetic field B. The V_H response results indicate that charge transport in the graphene is dominated by holes. As expected, the magnitude of V_H decreases when hole doping occurs after CN6-CP evaporation. The carrier areal density (n) is calculated from $n = IB/qV_H$, where q denotes the elemental charge. Following the equation, a high areal hole density in pristine graphene is estimated to be 8.3×10^{12} cm^{-2}. After 6 nm CN6-CP deposition, the areal hole density significantly increases to nearly 3 times up to 2.21×10^{13} cm^{-2}, demonstrating the strong p-type doping effect of CN6-CP to graphene.

In summary, effective surface charge transfer p-doping of graphene is realized by using a strong molecular acceptor CN6-CP. The *quasi in situ* UPS and XPS experiments on the electronic structure evolution at graphene/CN6-CP interface reveal that efficient and spontaneous electron transfer from graphene to CN6-CP

is responsible for the p-doping of graphene. Such an interfacial charge-transfer induced p-type doping of graphene leads to an upward band bending of 0.32 eV and an interface dipole of 1.09 eV. Consequently, the areal hole density of graphene significantly increases from 8.3×10^{12} cm^{-2} to 2.21×10^{13} cm^{-2} after 6 nm CN6-CP evaporation as confirmed by Hall effect measurements. The results indicate that CN6-CP can serve as a strong surface charge transfer dopant for graphene and holds a promise for broader applications in doping-related organic electronics.

Declaration of competing interest

The authors declare no competing financial interest.

Acknowledgments

This research was financially supported by the National Key Research and Development Program of China (No. 2017YFA0204700) and the National Natural Science Foundation of China (Nos. 21805285, 22175186 and 21803008).

References

[1] Z. Wang, A. Hemmetter, B. Uzlu, et al., Adv. Electron. Mater. 7 (2021) 2001210.
[2] J. Yang, P. Hu, G. Yu, APL Mater. 7 (2019) 020901.
[3] F. Bonaccorso, Z. Sun, T. Hasan, A.C. Ferrari, Nat. Photon. 4 (2010) 611–622.
[4] F. Su, S. Zheng, F. Liu, et al., Chin. Chem. Lett. 32 (2021) 914–917.
[5] M. Sun, C. Zhang, D. Chen, et al., SmartMat 2 (2021) 213–225.
[6] Z. Wang, K. Yi, Q. Lin, et al., Nat. Commun. 10 (2019) 1544.
[7] C.A. Di, D.C. Wei, G. Yu, et al., Adv. Mater. 20 (2008) 3289–3293.
[8] Y. Chu, B. Xi, S. Xiong, Chin. Chem. Lett. 32 (2021) 1983–1987.
[9] L. Cai, G. Yu, Small Methods 3 (2019) 1900071.
[10] L. Sun, K. Wang, N. Li, et al., Chin. Chem. Lett. 31 (2020) 2333–2338.
[11] L.P. Ma, Z. Wu, L. Yin, et al., Proc. Natl. Acad. Sci. U. S. A. 117 (2020) 25991–25998.
[12] X. Li, T. Sun, K. Zhou, et al., Nanotechnology 31 (2020) 315204.
[13] H. Wang, H.S. Wang, C. Ma, et al., Nat. Rev. Phys. 3 (2021) 791–802.
[14] C.G. Qiu, F. Liu, L. Xu, et al., Science 361 (2018) 387–391.
[15] A. Das, S. Pisana, B. Chakraborty, et al., Nat. Nanotech. 3 (2008) 210–215.
[16] R. Rong, S. Liu, Chin. Chem. Lett. 31 (2020) 565–569.
[17] H. Zhu, X. Gan, A. McCreary, et al., Nano Today 30 (2020) 100829.
[18] Y. Wu, X. Liu, D. Xia, et al., Chin. Chem. Lett. 31 (2020) 559–564.
[19] W.R.L.P. Ma, H.M. Cheng, Acta Phys. Chim. Sin. 38 (2022) 2012080.
[20] W. Chen, S. Chen, D.C. Qi, et al., J. Am. Chem. Soc. 129 (2007) 10418–10422.
[21] N. Liu, H. Tian, G. Schwartz, et al., Nano Lett. 14 (2014) 3702–3708.
[22] H. Liu, Y. Liu, D. Zhu, J. Mater. Chem. 21 (2011) 3335–3345.
[23] P. Rosenzweig, H. Karakachian, D. Marchenko, et al., Phys. Rev. Lett. 125 (2020) 176403.
[24] M. Kim, K.J. Kim, S.J. Lee, et al., ACS Appl. Mater. Interfaces 9 (2017) 701–709.
[25] X. Du, W. Jiang, Y. Zhang, et al., ACS Appl. Mater. Interfaces 12 (2020) 56361–56371.
[26] Z. Chen, I. Santoso, R. Wang, et al., Appl. Phys. Lett. 96 (2010) 213104.
[27] X. Zhang, Z. Shao, X. Zhang, et al., Adv. Mater. 28 (2016) 10409–10442.
[28] H. Kinoshita, I. Jeon, M. Maruyama, et al., Adv. Mater. 29 (2017) 1702141.
[29] L.P. Ma, S. Dong, M. Chen, et al., ACS Appl. Mater. Interfaces 10 (2018) 40756–40763.
[30] H. He, K.H. Kim, A. Danilov, et al., Nat. Commun. 9 (2018) 3956.
[31] T. Fukunaga, M.D. Gordon, P.J. Krusic, J. Am. Chem. Soc. 98 (1976) 611–613.
[32] T. Fukunaga, J. Am. Chem. Soc. 98 (1976) 610–611.
[33] Y. Karpov, T. Erdmann, I. Raguzin, et al., Adv. Mater. 28 (2016) 6003–6010.
[34] H.L. Smith, J.T. Dull, S.K. Mohapatra, et al., ACS Appl. Mater. Interfaces 14 (2022) 2381–2389.
[35] Y. Liu, B. Nell, K. Ortstein, et al., ACS Appl. Mater. Interfaces 11 (2019) 11660–11666.
[36] W.L. Xing, S.C. Wu, Y.Y. Liang, et al., ACS Appl. Mater. Interfaces 12 (2020) 29540–29548.
[37] S. Wu, X. Wu, W. Xing, et al., Macromol. Rapid Commun. 41 (2020) 1900322.
[38] W. Xing, J. Chen, Y. Liang, et al., RSC Adv. 9 (2019) 31840–31845.
[39] S.C. Wu, W.L. Xing, M.S. Zhu, et al., J. Mater. Chem. C 9 (2021) 4158–4163.
[40] Y. Karpov, N. Kiriy, P. Formanek, et al., Adv. Electron. Mater. 6 (2020) 1901346.
[41] J. Saska, G. Gonel, Z.I. Bedolla-Valdez, et al., Chem. Mater. 31 (2019) 1500–1506.
[42] Y. Karpov, N. Kiriy, M. Al-Hussein, et al., Chem. Commun. 54 (2018) 307–310.
[43] Y. Zou, H.Y. Mao, Q. Meng, D.B. Zhu, J. Chem. Phys. 144 (2016) 084706.
[44] W.R. Zhao, X.J. Dai, L.Y. Liu, et al., Appl. Phys. Lett. 118 (2021) 253302.
[45] Y. Zou, Q. Meng, H.Y. Mao, D.B. Zhu, Org. Electron. 41 (2017) 307–314.
[46] S. Braun, W.R. Salaneck, M. Fahlman, Adv. Mater. 21 (2009) 1450–1472.
[47] D.F. Yuan, D.Z. Huang, S.M. Rivero, et al., Chem 5 (2019) 964–976.
[48] C. Gaul, S. Hutsch, M. Schwarze, et al., Nat. Mater. 17 (2018) 439–444.
[49] X.J. Dai, Q. Meng, F.J. Zhang, et al., J. Energy Chem. 62 (2021) 204–219.
[50] B. He, T.W. Ng, M.F. Lo, et al., ACS Appl. Mater. Interfaces 7 (2015) 9851–9857.
[51] J.M. Ding, Z.T. Liu, W.R. Zhao, et al., Angew. Chem. Int. Ed. 58 (2019) 18994–18999.